The Astrophysical Journal, 779:98 (14pp), 2013 December 20 doi:10.1088/0004-637X/779/2/98

TWO SUPERLUMINOUS SUPERNOVAE FROM THE EARLY UNIVERSE DISCOVERED BY THE SUPERNOVA LEGACY SURVEY

D. A. Howell[1,2], D. Kasen[3,4], C. Lidman[5], M. Sullivan[6], A. Conley[7], P. Astier[8], C. Balland[8,9], R. G. Carlberg[10], D. Fouchez[11], J. Guy[8], D. Hardin[8], R. Pain[8], N. Palanque-Delabrouille[12], K. Perrett[13], C. J. Pritchet[14], N. Regnault[8], J. Rich[12], and V. Ruhlmann-Kleider[12]

[1] Las Cumbres Observatory Global Telescope Network, 6740 Cortona Drive, Suite 102, Goleta, CA 93117, USA
[2] Department of Physics, University of California, Santa Barbara, Broida Hall, Mail Code 9530, Santa Barbara, CA 93106-9530, USA
[3] Departments of Physics and Astronomy, University of California, Berkeley, Berkeley, CA 94720-7300, USA
[4] Nuclear Science Division, Lawrence Berkeley National Laboratory, 1 Cyclotron Road, Berkeley, CA 94720, USA
[5] Australian Astronomical Observatory, P.O. Box 915, North Ryde, NSW 1670, Australia
[6] School of Physics and Astronomy, University of Southampton, Southampton SO17 1BJ, UK
[7] Center for Astrophysics and Space Astronomy, University of Colorado, 389 UCB, Boulder, CO 80309-389, USA
[8] LPNHE, CNRS-IN2P3 and University of Paris VI & VII, F-75005 Paris, France
[9] University of Paris-Sud, Orsay, F-91405, France
[10] Department of Astronomy and Astrophysics, University of Toronto, 50 St. George Street, Toronto, ON M5S 3H8, Canada
[11] CPPM, CNRS-IN2P3 and University Aix Marseille II, Case 907, F-13288 Marseille Cedex 9, France
[12] DSM/IRFU/SPP, CEA-Saclay, F-91191 Gif-sur-Yvette, France
[13] DRDC Ottawa, 3701 Carling Avenue, Ottawa, ON K1A 0Z4, Canada
[14] Department of Physics and Astronomy, University of Victoria, P.O. Box 3055, Victoria, BC V8W 3P6, Canada
Received 2013 April 1; accepted 2013 September 19; published 2013 November 27

ABSTRACT

We present spectra and light curves of SNLS 06D4eu and SNLS 07D2bv, two hydrogen-free superluminous supernovae (SNe) discovered by the Supernova Legacy Survey. At $z = 1.588$, SNLS 06D4eu is the highest redshift superluminous SN with a spectrum, at $M_U = -22.7$ it is one of the most luminous SNe ever observed, and it gives a rare glimpse into the rest-frame ultraviolet where these SNe put out their peak energy. SNLS 07D2bv does not have a host galaxy redshift, but on the basis of the SN spectrum, we estimate it to be at $z \sim 1.5$. Both SNe have similar observer-frame $griz$ light curves, which map to rest-frame light curves in the U band and UV, rising in ∼20 rest-frame days or longer and declining over a similar timescale. The light curves peak in the shortest wavelengths first, consistent with an expanding blackbody starting near 15,000 K and steadily declining in temperature. We compare the spectra with theoretical models, and we identify lines of C II, C III, Fe III, and Mg II in the spectra of SNLS 06D4eu and SCP 06F6 and find that they are consistent with an expanding explosion of only a few solar masses of carbon, oxygen, and other trace metals. Thus, the progenitors appear to be related to those suspected for SNe Ic. A high kinetic energy, 10^{52} erg, is also favored. Normal mechanisms of powering core-collapse or thermonuclear SNe do not seem to work for these SNe. We consider models powered by ^{56}Ni decay and interaction with circumstellar material, but we find that the creation and spin-down of a magnetar with a period of 2 ms, a magnetic field of 2×10^{14} G, and a 3 $M_\odot$ progenitor provides the best fit to the data.

Key word: supernovae: general

Online-only material: color figures

1. INTRODUCTION

Barbary et al. (2009) announced the discovery of an unusual, unexplained transient in the course of the Supernova Cosmology Project cluster supernova (SN) search. With no apparent host galaxy, the redshift was undetermined. The event had spectra with broad, unexplained absorption lines and a light curve in the observed i and z bands that rose to maximum over 100 days and declined on a similar timescale. Soon after, we noticed two similar, puzzling transients in the Supernova Legacy Survey (SNLS; Perrett et al. 2010), SNLS 06D4eu[15] and SNLS 07D2bv, with rise times in i and z bands >80 days, no obvious host or redshift, and unexplained, broad-lined spectra.

The key to decoding these mystery objects was found with the discovery of several new unexplained transients in the course of the Palomar Transient Factory (PTF; Law et al. 2009). Quimby et al. (2011) determined that the new PTF transients and SCP 06F6 were related to SN 2005ap, an exceptionally luminous SN previously discovered during the course of the Texas Supernova Search at $z = 0.2832$ that reached an absolute magnitude (unfiltered) of −22.7 (Quimby et al. 2007). By coadding all the spectra of SCP 06F6, Quimby et al. (2011) detected weak host galaxy Mg II lines and determined the redshift to be $z = 1.189$. Thus, the mysterious lines in the optical spectra of SCP 06F6 had never before been seen because they were from the rest-frame ultraviolet of the SN. Furthermore, this explained the puzzling, seemingly physically implausible long rise (Chatzopoulos et al. 2009) of the light curve of SCP 06F6—it was due to $1 + z$ time dilation.

Essential to finding link between SN 2005ap and SCP 06F6 were four similar transients discovered by PTF: PTF09cnd, PTF09cwl, PTF09atu, and PTF10cwr (Quimby et al. 2011). Because some were at intermediate redshifts, they had spectra bridging the rest-frame optically dominated SN 2005ap and the rest-frame UV-dominated SCP 06F6. They also had a rise to maximum light of 20–50 days, had no hydrogen in the spectra, were UV-bright, and were exceptionally luminous, with peak rest-frame u-band (AB) magnitudes < -21. One of these SNe,

[15] Each SNLS candidate is given a name that consists of the name of the survey, the year it was discovered, the field in which it was found, and a running index consisting of two letters. Hence, SNLS 06D4eu was the 125th candidate to be found in the D4 field during 2006.

PTF10cwr, also known as SN 2010gx, was also followed by the Pan-STARRS1 (PS1) survey (Pastorello et al. 2010). The time-series spectra from Quimby et al. (2011) and Pastorello et al. (2010) reveal that, though early-time spectra of this class of objects do not resemble hydrogen and helium-poor SNe Ic, late-time spectra do. At early times, spectra reveal a blue continuum with a quintuplet of O II lines in the rest-frame optical and lines tentatively identified as Si III, Mg II, and C II in the UV (Quimby et al. 2011). Spectra and light curves are consistent with a blackbody with $T \sim 15{,}000$ K at early times, cooling as it expands.

The extraordinary luminosity of these events, of the order of 10 times brighter than a thermonuclear SN Ia and 100 times brighter than a typical core-collapse SN, is difficult to explain. The light curve of an SN Ia is powered by the radioactive decay of $\sim$0.6 $M_\odot$ of ^{56}Ni synthesized in the explosion. Core-collapse SNe are generally powered by a combination of smaller amounts of radioactive material and the energy of gravitational collapse deposited in what were formerly the outer layers of the expanding star. Neither of these mechanisms seems capable of explaining the extreme luminosity of these SNe. In the first case, their light curves do not have the characteristic rise and fall time associated with ^{56}Ni decay. In the second case, since the energy is deposited in a small radius, which is then lost to adiabatic expansion, such extreme luminosities at relatively late times are not possible.

One class of core-collapse SNe, SNe IIn, can attain exceptional luminosities ($M_V < -21$) by the interaction between the ejecta and preexisting circumstellar material (CSM) cast off by the progenitor. This is possible because there is additional energy input at relatively late times, after the ejecta has expanded. However, the telltale signature, narrow hydrogen lines in the spectra, are not seen for the class of superluminous supernovae (SLSNe) covered here. One possibility is that the previous cast-off material is not hydrogen-rich but is instead a shell of carbon and oxygen lost in a previous pulse of a pulsational pair-instability SN (Woosley et al. 2007; Quimby et al. 2011), although the existence of such phenomena is speculative.

Another possibility for powering these SNe comes from the birth and spin-down of a magnetar (Kasen & Bildsten 2010; Woosley 2010). In this model, a highly magnetized, rapidly spinning neutron star is created in the SN. It rapidly loses energy, decreasing its spin period, and transfers some of it to the expanding SN ejecta. While the required energies are achievable, it is not clear how the energy from the spin-down would be coupled to the nascent SN nor (until now) what the spectra or light curves of such events would look like.

We can hope to gain some insight into the physical mechanism surrounding SLSNe by examining their stellar environments. Neill et al. (2011) found that these events generally favor UV-bright, blue hosts with a low mass and high star formation rate (SFR). For a review of all properties of SLSNe, including hydrogen-rich events, see Gal-Yam (2012).

Here we present data on the two SLSNe with spectra from the SNLS: SNLS 06D4eu and SNLS 07D2bv. One of these, 06D4eu, has an accurate redshift from its host galaxy, allowing an accurate determination of its luminosity. Therefore, we use it as a case study, comparing it with theoretical models, including new work on the magnetar spin-down model of Kasen & Bildsten (2010). The paper is divided as follows. In Section 2, we summarize key aspects of the SNLS survey and describe how two SLSNe, SNLS 06D4eu and SNLS 07D2bv, were discovered there. In Section 3, we present Very Large Telescope (VLT)/X-Shooter observations that enable us to derive the redshift and SFR of the likely host of SNLS 06D4eu. In Section 4, we present the light curves and fit them with blackbody models. In Section 5, we present the spectra and fit them with a radiative transfer model to identify features. In Section 6, we try to explain the luminosity of SNLS 06D4eu by using models, and we discuss progenitor scenarios. Finally, we conclude in Section 7. Throughout the paper we use Vega magnitudes unless otherwise noted, and we assume a flat lambda-dominated Universe with $\Omega_M = 0.27$ and $H_0 = 71$ km s^{-1} Mpc^{-1}.

2. DISCOVERY

2.1. The Supernova Legacy Survey

The SNLS was designed to constrain the dark-energy equation-of-state parameter by using distances and redshifts of several hundred spectroscopically confirmed Type Ia supernovae (SNe Ia). The SNLS comprised two parts: an imaging part that was based on the Deep Survey of the Canada–France–Hawaii Telescope Legacy Survey[16] (CFHT-LS) and a spectroscopic part that was designed to follow up SN candidates that were discovered in the imaging survey.

The imaging survey consisted of regular imaging of four fields, labeled D1–D4, in the four filters: *g*, *r*, *i,* and *z*. Each field was observed once every three to five nights on and around new moon. This technique for finding transients, which is often referred to as the "rolling search" technique, naturally leads to well-sampled, multicolored light curves Over the 5 years during which the survey ran, the light curves of approximately 1000 SNe Ia and many other variable sources were obtained. Details of the real-time observing strategy and follow-up can be found in Perrett et al. (2010). Three year results are published in Guy et al. (2010), Conley et al. (2011), and Sullivan et al. (2011).

The spectroscopic follow-up for the SNLS was done with several instruments: GMOS on Gemini North and Gemini South (Howell et al. 2005; Bronder et al. 2008; Walker et al. 2011), LRIS and DEIMOS on the Keck I and Keck II telescopes (Ellis et al. 2008), and FORS1 and FORS2 on VLT Antu and Kueyen (Balland et al. 2009).

Light curves and spectra from this paper will be made available via the WISeREP repository (Yaron 2012).

2.2. SNLS 06D4eu

SNLS 06D4eu was discovered in images taken on 2006 August 20 (UT), processed with the real-time processing pipeline (Perrett et al. 2010), at $i = 23.7$. It was subsequently recovered on prior imaging going back to 2006 July 27. The field of SNLS 06D4eu is shown in Figure 1.

As part of the regular follow-up of SNLS candidates, SNLS 06D4eu (R.A. 22:15:54.291, decl. −18:10:45.56 J2000) was submitted to the ESO VLT for spectroscopic confirmation. At this stage, it was flagged as a rank B candidate, i.e., it was thought to be an SN Ia on the basis of early premaximum light curve data, but there were some anomalies in the early part of the light curve that prevented it from being classified as a rank A candidate.

Soon after the request was submitted, SNLS 06D4eu was observed with the Mutli-Object Spectroscopy (MOS) mode of FORS1 on 2006 August 31. FORS1 was used with the 300V grism in conjunction with the GG435 order sorting filter. The slit width was set to 1″, which results in a spectral resolution of

[16] http://www.cfht.hawaii.edu/Science/CFHLS/

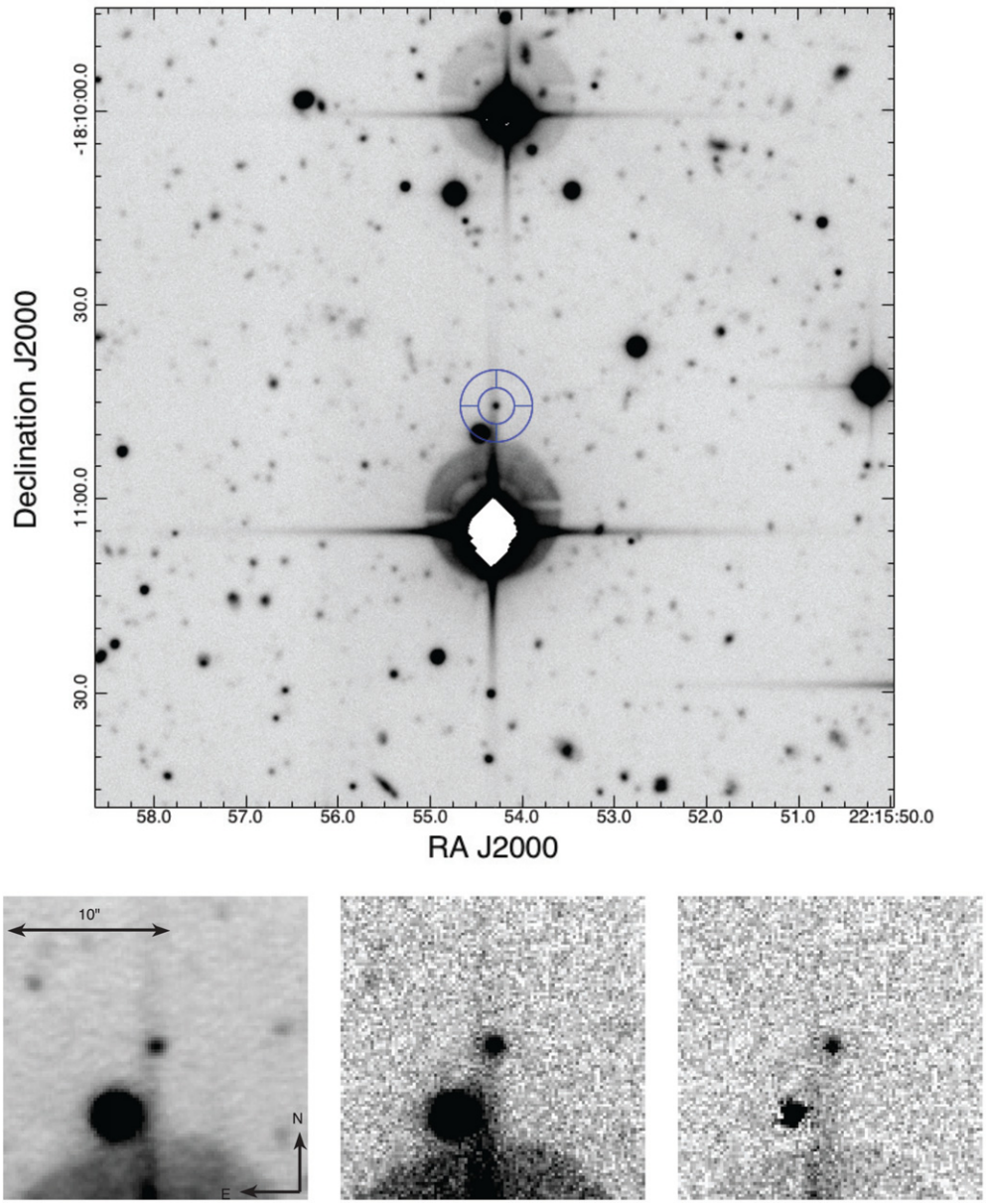

Figure 1. Top: CFHT MegaCam image centered on SNLS 06D4eu. This cutout is 2 arcmin on a side, and north is up and east left. The position angle of the X-Shooter slit was aligned so that scattered light from the 13th magnitude star that is only 20″ south of SNLS 06D4eu did not contaminate the spectrum. Bottom: the image detection triplet, which from left to right shows the reference image, an image of SNLS 06D4eu when it was close to maximum light, and the difference between the first two. The images were taken in the *g* band.

(A color version of this figure is available in the online journal.)

400. The resulting spectrum (Figure 2) starts around 4250 Å and ends at approximately 8500 Å. The exposure time was 4500 s and was split into five exposures of 900 s each.

The FORS1 data were processed with standard IRAF routines.[17] The detector bias was removed by fitting a low order polynomial to the overscan region. Pixel-to-pixel sensitivity variations were removed by using an image of a uniformly illuminated white screen. The spectrum of SNLS 06D4eu was then extracted and calibrated in wavelength and flux.

The advantage of the MOS mode is that, in addition to obtaining a spectrum of SNLS 06D4eu, the MOS mode allows us to target other objects such as the host galaxies of transients, many of them SNe for which we could not get a spectrum when they were bright. Toward the end of the SNLS project, typically 5 of the 19 MOS slits could be placed on such targets. The remaining slits were placed on randomly chosen field galaxies.

The MOS data were processed one month after the data were taken; however, we failed to appreciate the interesting nature of the SN spectrum until 8 months later (no such SN had ever been identified at that point), so we lost an opportunity to follow it spectroscopically and at other wavelengths.

Fortunately, SNLS was a rolling search, meaning that each field was repeatedly imaged to search for new SNe while building light curves of previously detected events. Therefore, as for all transients, *griz* light curves of SNLS 06D4eu were obtained by default and could be analyzed in retrospect. This light curve is shown in Figure 3 and discussed in detail in Section 4.

[17] IRAF is distributed by the National Optical Astronomy Observatory, which is operated by the Association of Universities for Research in Astronomy, Inc., under cooperative agreement with the National Science Foundation.

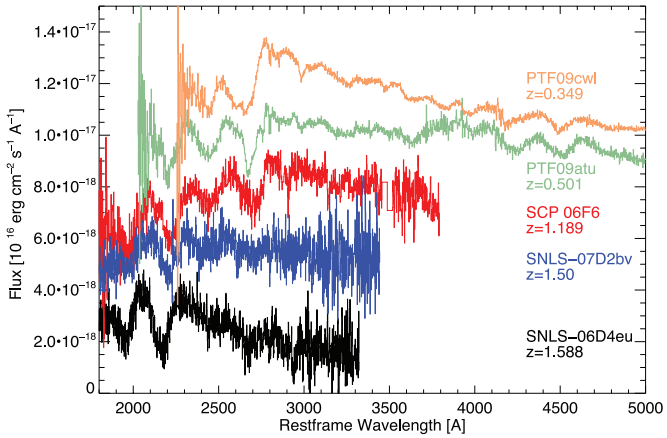

Figure 2. Spectra of SNLS 06D4eu and SNLS 07D2bv compared with other similar events in the rest frame (Quimby et al. 2011; Barbary et al. 2009). SNLS 06D4eu extends farthest to the rest-frame UV because it is the highest redshift. The overall shape of the spectrum also peaks near 2000 Å, in contrast to the other events. This bluer color is likely because the spectrum was taken earlier than the other events. Note that the absorption feature near 2200 Å is strongest in SNLS 06D4eu. Additionally, an absorption feature near 1900 Å, seen in SCP 06F6, is apparent in SNLS 06D4eu. SNLS 07D2bv is shown at a redshift of $z = 1.50$, although this is approximately determined from matching its features with SNLS 06D4eu; no host galaxy redshift could be obtained. We show the second of three spectra obtained for SCP 06F6. The first does not extend far enough to the blue to make a meaningful comparison, and the third is not substantially different from the second.

(A color version of this figure is available in the online journal.)

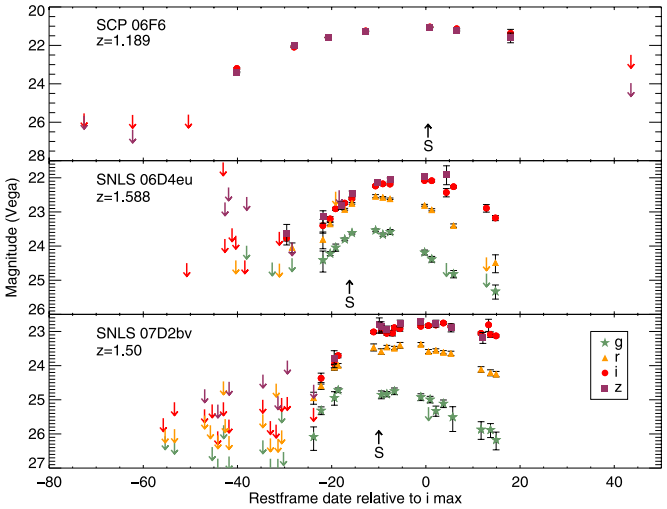

Figure 3. Light curves of SCP 06F6, SNLS 06D4eu, and SNLS 07D2bv. Observed magnitudes are shown in the Vega system, although the time axis has been corrected for $1 + z$ time dilation. An "S" with an arrow denotes when the spectra shown in Figure 2 were taken. Downward arrows denote 3σ upper limits.

(A color version of this figure is available in the online journal.)

Just as for SCP 06F6, from the initial spectrum (Figure 2) the redshift of SNLS 06D4eu was unclear. We attempted to spectroscopically observe the host galaxy in the optical after the SN faded, but we did not detect host galaxy lines. Ultimately, a multihour VLT X-Shooter spectrum showed emission lines in the IR, revealing the redshift to be 1.588 (Section 3).

2.3. SNLS 07D2bv

SNLS 07D2bv (Figure 4) was discovered on 2007 February 22 by the SNLS (at $i = 24$ according to real-time photometry) but was then detected at 5σ or greater on prior images beginning on February 9. The light curve is shown in Figure 3.

It was categorized as a class "C" candidate, meaning it was unlikely, but possible, to be an SN Ia. As a result of its low priority, a spectrum was not obtained until March 16, when it was observed by VLT FORS1 in MOS mode, by which time the SN had risen to ≈23 mag in the z band. The spectrum is shown in Figure 2. The setup and data reduction are identical to that mentioned above for SNLS 06D4eu, but the exposure time was 4×900 s. The one-hour spectrum revealed broad SN-like features, with no apparent host lines, and was eventually noted as "06D4eu-like." Because of the faintness of the four nearby potential host galaxies, it was not possible to obtain subsequent host galaxy spectroscopy.

Table 1
X-Shooter Setup

Arm	Slit width × length	Res.[a]	Integration (2009) (s)	Integration (2010) (s)
UVB	1.″0 × 11″	5000	9000	7200
VIS	0.″9 × 11″	9000	9000	7200
NIR	0.″9 × 11″	5000	8640	7200

Note. [a]The resolution is set by the slit.

3. THE HOST OF SNLS 06D4eu

3.1. Observations with X-Shooter

Spectra of the host of SNLS 06D4eu covering 300–2500 nm were obtained with X-Shooter/Kueyen during 2009 and 2010 (Figure 5). X-Shooter (D'Odorico et al. 2006) consists of three arms: an ultraviolet-blue arm (UVB) covering the 300–550 nm spectral region, a visible arm (VIS) covering the 550–1000 nm spectral region, and a near-infrared arm (NIR) covering the 1000–2500 nm spectral region. Each arm has its own cross-dispersed spectrograph and detector. The light from the target is split between the three arms by two dichroics. The configuration of X-Shooter that was used to observe the host of SNLS 06D4eu is listed in Table 1.

The position angle of the instrument was set so that scattered light from the bright star that is located 20″ to the South of SNLS 06D4eu (see Figure 1) would not contaminate the spectrum of the host of SNLS 06D4eu. During the observations, the sky was clear and the seeing, as measured by the site seeing monitor, averaged around 0.″8.

To facilitate the removal of the NIR background and to mitigate the effect of the large number of hot pixels in the NIR detector, the target was offset between two positions along the echelle slit. During 2009, the frequency of the offsetting was once every ∼1600 s, during which three 480 s exposures in the NIR arm and one 1500 s exposure in each of the UVB and VIS arms were taken. Already, from the data taken in 2009, lines from [O II], [O III], and Hα could be detected in the data. However, Hβ landed in a region that was contaminated with bright night sky lines, so a secure detection of Hβ could not be made. At that stage, the target was only visible during the beginning of the night, which is when night sky lines are bright and variable. We suspended the program for six months so that the target could be observed toward the end of the night when night sky lines are considerably fainter. We also increased the offset frequency to once every ∼300 s and took one 300 s exposure in each of the arms at each offset position. These data were taken in 2010.

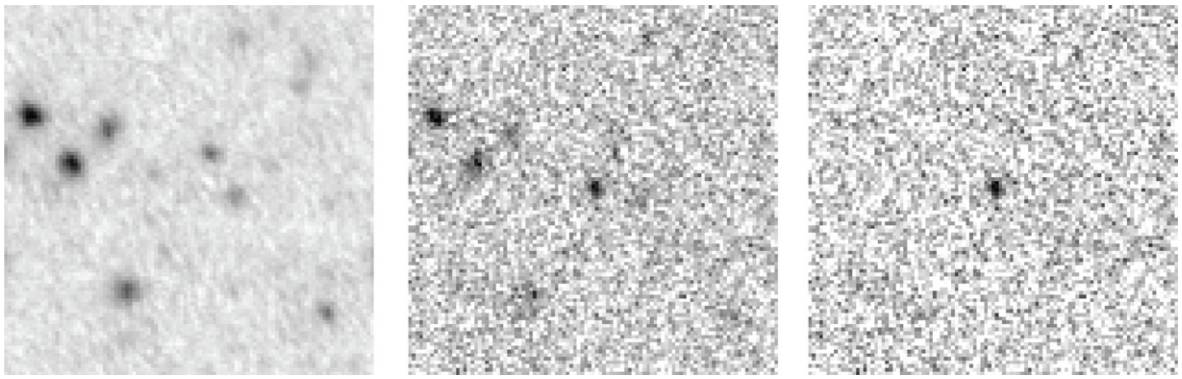

Figure 4. Detection triplet for SNLS 07D2bv. The leftmost image is the reference image, created by stacking SNLS data from years in which the supernova did not appear. The middle image shows the supernova (center) after it started to brighten. The right image is a subtraction showing the discovery of the supernova. The scale is the same as in Figure 1

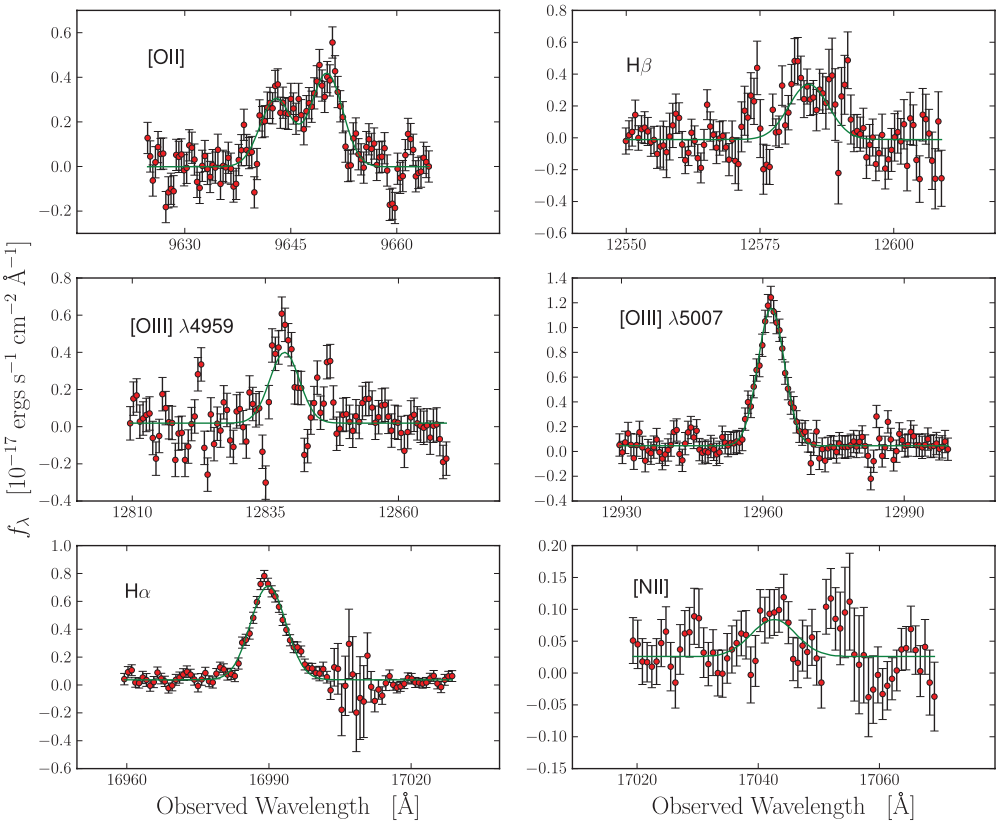

Figure 5. Six emission lines detected in the host galaxy of SNLS 06D4eu together with a Gaussian fit (green line). The [O II] λλ3727,3729 doublet is fitted with two Gaussians. The line fluxes reported in Table 2 are determined by integrating the area under the fits.

(A color version of this figure is available in the online journal.)

The increased offset frequency allowed us to remove the OH and O_2 lines near Hβ better. The visibility of Hβ was also helped by Earth's motion around the sun. The resulting Doppler shift moved Hβ away from the brightest O_2 line. The total integration times for the 2009 and 2010 observations are reported in Table 1.

Both the VIS and NIR arms were processed in an identical manner. Consecutive images were grouped into pairs, which consisted of images that were taken on either side of the offset. Within each pair, one image was subtracted from the other. This results in a frame in which the object appears twice: once with positive counts and again with negative counts. While this method removes most of the background, significant residuals remain, and an additional step to remove these residuals was necessary.

The tilt of the path that traces the spatial direction changes noticeably as one moves along an order, and this adds some complexity to the removal of the residuals. At this point, one can choose to rectify the spectrum and proceed with removing the residuals or, as we do, compute the residual along a path that follows the spatial direction. For this, we used our own custom made software. The latter avoids interpolation, which introduces correlations between pixels and tends to grow the region over which bad pixels, which are quite common with the current NIR detector of X-Shooter, can affect the data. For the UVB arm, the sky background was removed from all images directly.

Apart from the removal of the sky background, the processing of the data was standard, and we used IRAF for most of the processing tasks. For all arms, two spectra, offset by the

Table 2
Observed Line Fluxes of the Host of SNLS 06D4eu

Line	Observed Line Flux (10^{-17} erg s^{-1} cm^{-2})
[O II] λλ3727,3729	$4.0^{+0.6}_{-0.7}$
Hβ	$3.3^{+0.4}_{-0.3}$
[O III] λ4959	$2.7^{+0.3}_{-0.3}$
[O III] λ5007	$7.8^{+0.7}_{-0.5}$
Hα	$6.3^{+0.4}_{-0.4}$
[N II] λ6584	$0.55^{+0.10}_{-0.15}$

nod throw, were extracted. All spectra were then wavelength calibrated. Where there were sufficient night sky lines (all of the NIR and most of the VIS), we used night sky lines to do the wavelength calibration. Otherwise we used arc frames. A star with spectral type B9V was used to remove telluric features and to calibrate the flux scale. As a final step, all spectra were then corrected to the heliocentric reference frame.

3.2. The Redshift of the Host of SNLS 06D4eu

The X-Shooter spectrum of the host SNLS 06D4eu shows several clear emission lines, such as [O II] λλ3727,3729, Hβ [O III] λλ4959,5007, and Hα (Figure 5). They lead to a host redshift of $z = 1.5881 \pm 0.0001$.[18] The [O II] doublet is resolved, and both components of the [O III] doublet are detected. The fluxes of all lines are listed in Table 2. We tentatively detect [N II] λ6584 in the two-dimensional sky-subtracted data. However, the detection is marginal (only 4σ), and the relative uncertainty in the derived flux is large.

Most lines land in regions that are relatively free of bright night sky lines and telluric features. The [O II] λλ3727,3729 doublet is slightly contaminated by both, but neither the sky lines nor the telluric absorption features near the doublet are strong enough to bias the flux measured for [O II]. Hβ lands close to a bright night sky line. It is more clearly separated from the line in the 2010 data, due to the motion of the Earth around the Sun, so we only use the 2010 data when estimating the Hβ line flux. The continuum is detected but only in the VIS and UVB arms. It is clearest in the UVB arm; however, the signal-to-noise ratio is low, and absorption features cannot be seen.

The lines detected in the X-Shooter spectrum land in regions that lie outside the wavelength intervals that were covered in earlier attempts to get the host redshift by using GMOS on Gemini South and FORS2 on the VLT.

3.3. Dust Extinction, Star Formation Rate and Metallicity

Derived quantities from host galaxy lines are summarized in Table 3.

An estimate of the amount of extinction from dust can be made by comparing the measured Hα to Hβ line ratio with the theoretical value, which for case-B recombination is 2.86 (Osterbrock 1989). We measure $1.9^{+0.3}_{-0.2}$, a value that is slightly lower than the theoretical value. The difference is opposite to what one expects to occur if there is extinction from dust, so we conclude that there is no evidence for significant extinction and posit that the emission lines and the quantities computed from them are unaffected by dust.

[18] The redshift is in the heliocentric frame.

Table 3
Derived Quantities from Host Lines

Indicator	Value
Hα/Hβ	$1.9^{+0.3}_{-0.2}$
SFR(Hα)	$8.3 \pm 0.3\ M_\odot\ \mathrm{yr}^{-1}$
[N II]/[O II]	0.14 ± 0.04
[N II]/Hα	0.09 ± 0.02
R_{23}	$4.4^{+0.6}_{-0.5}$
O_{32}	$2.6^{+0.6}_{-0.4}$
12+log(O/H) [lower]	7.9
12+log(O/H) [upper]	8.9
[N II] λ6584	$0.55^{+0.10}_{-0.15}$

Following Kennicutt (1998), we use the Hα line flux to derive the SFR of the host of SNLS 06D4eu. The Hα flux translates to a SFR of $8.3 \pm 0.3\ M_\odot\ \mathrm{yr}^{-1}$, which means that the host of SNLS 06D4eu is vigorously forming stars.

Estimating the metallicity of the gas from emission lines is more problematic. The R_{23} index (Pagel et al. 1979), which uses [O II], [O III], and Hβ, is sensitive to the gas phase metallicity and q, the ionization parameter (Kobulnicky & Kewley 2004). The index is also doubly valued, i.e., for one value of R_{23}, two metallicities are possible. The two values are usually referred to as the upper and lower branches. Hence, using it to derive the metallicity requires one to decide which branch to use. This requires additional information, such as the [N II] λ6584 to Hα line ratio (Kobulnicky & Kewley 2004) or the [N II] λ6584 to [O II] line ratio (Kewley & Ellison 2008), for which we derive 0.09 ± 0.02 and 0.14 ± 0.04, respectively. The [N II]/[O II] ratio indicates that the upper branch should be used; however, given the uncertainty in the ratio, we cannot exclude the possibility that the lower branch should be used instead. Deeper spectra are needed to answer this question.

Kobulnicky & Kewley (2004) recommend an iterative approach to computing the metallicity using both R_{23} and O_{32}. The O_{32} index is sensitive to both metallicity and to the ionization parameter. For the host galaxy of SNLS 06D4eu, we find $R_{23} = 4.4^{+0.6}_{-0.5}$ and $\mathrm{O}_{32} = 2.6^{+0.6}_{-0.4}$, which corresponds to a gas phase metallicity of $12 + \log(\mathrm{O/H}) = 8.9(7.9)$ if the galaxy lands on the upper (lower) branch.[19] For reference, the solar value is $12 + \log(\mathrm{O/H}) \sim 8.7$.

We do not attempt to derive a host galaxy mass for SNLS 06D4eu, because of a lack of long wavelength data. We do not have any data on the host redward of the 4000 Å break, since all observed optical data correspond to the rest-frame UV. Furthermore, no observed IR data exist. The WIRCAM data of the D4 field (Bielby et al. 2010) do not cover the SN position, and the VISTA hemisphere survey (McMahon 2012) has not yet targeted this area.

4. LIGHT CURVES

The observed ∼80 day rise times in the i and z bands for SNLS 06D4eu and SNLS 07D2bv were initially puzzling, as SNe powered by radioactive decay have a much shorter rise (e.g., ∼20 days for SNe Ia), and those powered by collisions with CSM stay at a fairly constant luminosity, e.g., SNe IIn. This mystery was resolved with the determination of the redshift of SNLS 06D4eu—because of $(1 + z)$ time dilation, the rest-frame

[19] For reference, the oxygen abundance, $12 + \log(\mathrm{O/H})$, is related to the metal mass fraction by $Z = 29 \times 10^{[12+\log(\mathrm{O/H})]-12}$ (Kobulnicky & Kewley 2004).

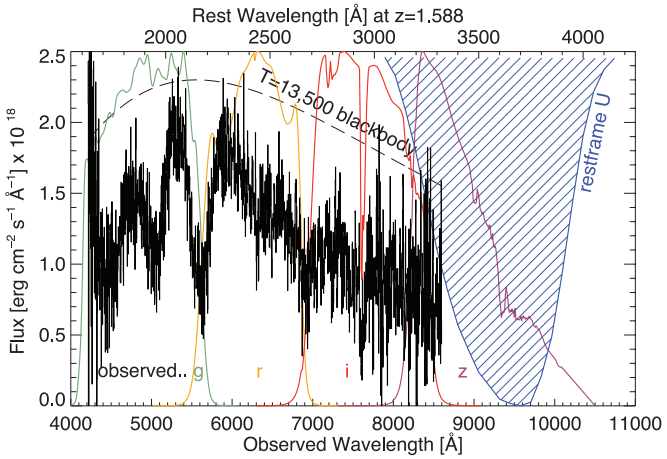

Figure 6. Spectrum of SNLS 06D4eu at observed and rest-frame wavelengths. CFHT Megacam filter bandpasses, used to collect the photometry in Figure 3, are indicated. Rest-frame U band is plotted upside down to indicate that it corresponds to the upper axis. It is a good match to observed z'. Note that g', r', and i' correspond to rest-frame ultraviolet regions of the spectrum. The overall shape of the spectrum is consistent with a $T = 13{,}500$ K blackbody. This is consistent with, and independent evidence of, the high temperatures indicated in the simple blackbody model fit to the photometry as discussed in Section 4.1.

(A color version of this figure is available in the online journal.)

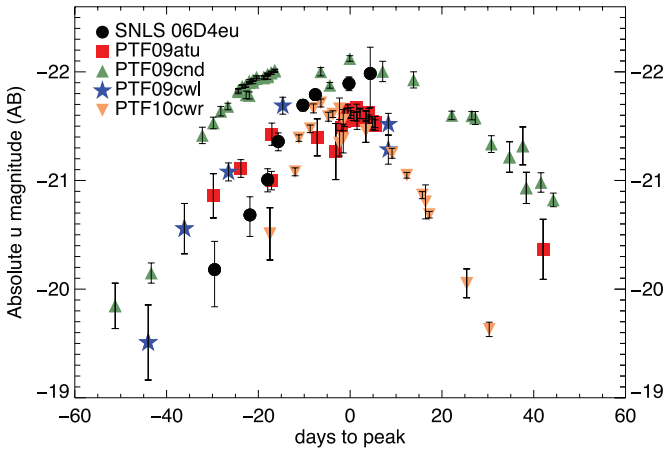

Figure 7. Absolute rest-frame u' magnitudes of SLSNe in the AB system. SNLS 06D4eu data are k-corrected from observed Megacam z-band data to SDSS u' by using the blackbody fit as the SED. Comparison SNe are from Quimby et al. (2011). Magnitudes are ∼0.7 brighter in the Vega system. SNLS 06D4eu is similar to the brightest of the SLSNe but has a shorter rise to maximum light, around 30 days. The time of peak is uncertain to about five days because of the large error on the final point. The PTF SNe have an uncertainty of several tenths of a magnitude due to k-correction uncertainties (R. M. Quimby 2012, private communication).

(A color version of this figure is available in the online journal.)

rise time is in fact much shorter, around 30 days (Figure 3) in the reddest observed bands.

In fact, because of the high redshift, the Megacam bands are sampling exclusively UV and U-band light. Figure 6 shows that observer-frame z corresponds to rest-frame U for SNLS 06D4eu. The g, r, and i light curves are sampling rest-frame bands centered near 1900 Å, 2400 Å, and 2900 Å, respectively. Thus, Figure 3 is remarkable in that it shows for the first time the entire near-UV light curve evolution for two SLSNe. It is apparent that these SNe are exceptionally UV-bright and blue at early times. The SN peaks in the observed g band (rest 1900 Å) and r band (rest 2400 Å) about 5–12 days before the rest-frame U band, earlier for SNLS 06D4eu and later for SNLS 07D2bv.

Before day −15 the colors of the SNe are fairly constant, but they rapidly become red as maximum light in the rest-frame U band is approached. After the peak, the colors return to a fairly constant value. This can be seen in Figure 3, although we do not include a separate color evolution figure because of the difficulty of k-correction to undefined UV filters and an unknown underlying spectral energy distribution (SED) evolution.

For SNLS 06D4eu, we k-correct the observed z data to rest-frame u to compare with other SLSNe from Quimby et al. (2011), as shown in Figure 7. The k-correction (Kim et al. 1996) requires the underlying SED as input. Since a representative time series of spectra for SLSNe is not known (nor whether they behave similarly enough to make this feasible), instead we fit a blackbody model to the photometry (Section 4.1) and use this as the SED for the k-correction. Figure 7 shows that SLSNe have diverse behavior in the u band. SNLS 06D4eu reaches a peak magnitude of −22 (AB), or −22.7 (Vega), comparable to the most luminous SLSNe although its rise time is relatively short. Note that because of the considerable uncertainties associated with the k-correction for SLSNe, the u-band magnitudes for the PTF objects in Figure 7 are uncertain by several tenths of a magnitude (R. M. Quimby 2012, private communication). K-corrections for SNLS 06D4eu are less uncertain, but because of the use of a blackbody model for the SED, they are probably not better than a tenth of a magnitude. SNLS 06D4eu is thus comparable in absolute magnitude to the most luminous hydrogen-poor SLSN, SN 2005ap ($M = -22.7$), according to Gal-Yam (2012).

4.1. Blackbody Fits

We can explain the behavior of the light curve as an expanding photosphere radiating as a cooling blackbody. For SNLS 06D4eu, for each day where we have four-band ($griz$) photometry taken within 24 hr, we fit a blackbody to the measured fluxes, as shown in Figure 8. At 22 days before peak brightness the SN is at $T \sim 15{,}000$ K, decreasing to around 10,600 K near maximum light. For the radius of the photosphere, at −21.8 days we find 1.7×10^{15} cm. Unfortunately, the SN had been detected for about a week before this date, and this large radius does not allow us to differentiate between possible progenitor models. At maximum light the best-fit radius was 6.1×10^{15} cm.

To make better use of all the data (not just those epochs with four-band photometry), we assume a simple model: expansion with the temperature decreasing linearly with time. The radius of the photosphere is given by

$$R(t) = R_0 + \frac{dR}{dt}t,$$

where R_0 is the initial radius, dR/dt is the rate of change of the position of the photosphere with time, and t is time in days. Meanwhile, the temperature evolution is given by

$$T(t) = T_0 - \frac{dT}{dt}t,$$

where T is the temperature in Kelvin, and T_0 is the initial temperature. Figure 9 shows a fit of this simple model to the data, and the best-fit parameters are given in Table 4. At day −30, the SN starts with $T \sim 16{,}000$ K, and the temperature decreases by about 200 K day^{-1}.

Considering the simplicity of the model, the fit to the photometry is quite remarkable. It correctly fits the colors of

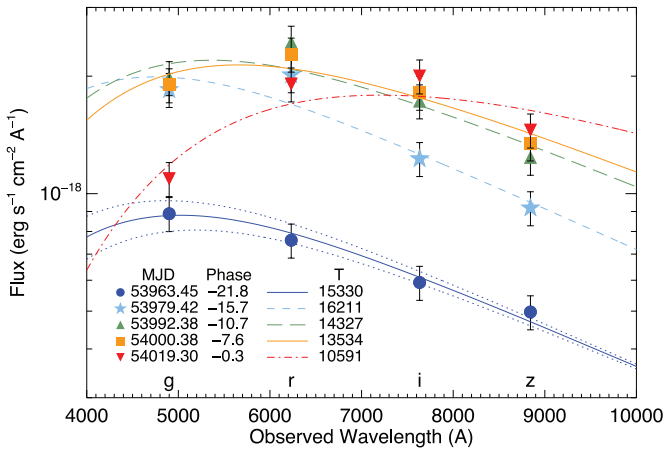

Figure 8. Blackbody fits to the photometry for SNLS 06D4eu on each day where 4 bands of photometry were available. Data points are located at the central wavelength of each filter. Only dates where all four bands were taken within 24 hr were considered. The flux from each day is fit independently for the radius of the emitter and the temperature of the blackbody. On rest-frame day −22 the SN was greater than 15,000 K (solid line), but by maximum light it had cooled to ≈10,600 K (dot-dashed line). Since the SN is not a perfect blackbody, Poisson errors underrepresent the true error on the blackbody fit. χ^2/dof of order unity is obtained with errors that are 10% of the flux (shown). The temperatures are relatively insensitive to the error model. The dotted line shows the effect of varying the temperature by ±500 K while keeping the radius fixed. It is only shown for the first epoch for clarity, though other phases are similar. Formally, the temperature is higher on day −15.7 compared with day −21.8, but this is likely because the observations are on the Rayleigh–Jeans tail for this phase, and the true temperature cannot be discerned accurately.

(A color version of this figure is available in the online journal.)

Table 4
Best-fit Parameters for Simple Blackbody Model

R_0	2.7
(dR/dt)	1.03 day^{-1}
T_0	16270 K
(dT/dt)	186 K day^{-1}

Note. Radii are relative.

the light curves and the relative timing of the peaks in each band. In other words, each light curve is not fit independently, they are all fit at once with the colors set by the model. The model is a relatively poor fit to the light curve at the earliest times and in the r band. Of course, given the relatively strong, broad lines in the spectrum, no blackbody fit is expected to be perfect.

The earliest data point in the r, i, and z bands deviates significantly from the simple model. This may indicate that the SN does not follow a simple blackbody at the earliest times. Some core-collapse SNe have an initial decrease in the light curves from the SN shock breaking out of the progenitor star, before they start to rise. However, Leloudas et al. (2012) saw an unexplained plateau that could not be explained by shock breakout in the early phase of the light curve for the SLSN SN 2006oz. With only one epoch's data deviating from a very simple model, we do not speculate further on the cause.

4.2. Energy Requirements

The peak absolute magnitude in rest-frame U is $M_U = -22.7 \pm 0.1$ (Vega), making SNLS 06D4eu among the most UV-luminous SN ever discovered.

From the blackbody fit, we derive an approximate bolometric peak luminosity of 3.4×10^{44} erg s^{-1}. Since we can only sample

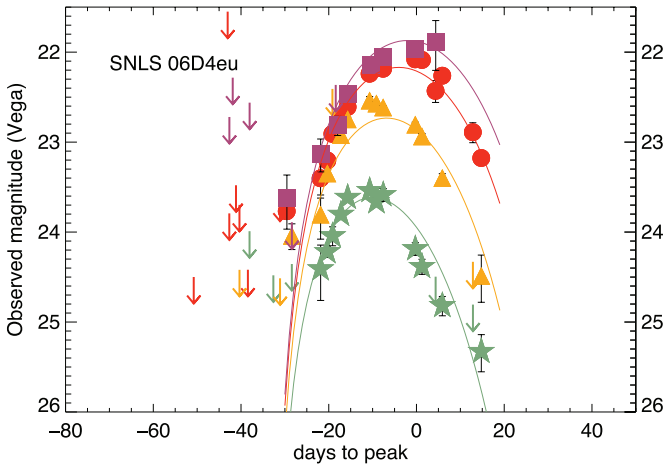

Figure 9. Points are photometry of SNLS 06D4eu as in Figure 3. Solid lines are the simple blackbody model described in Section 4.1, which has a linearly increasing radius and linearly increasing temperature. Parameters of this model are given in Table 4. The time axis is given in the rest frame.

(A color version of this figure is available in the online journal.)

the ultraviolet part of the SED, there is considerable uncertainty in using the blackbody assumption to extrapolate to a bolometric luminosity. However, the total radiated energy is approximately 10^{51} erg (1 Bethe [B]), comparable to that of other hydrogen-poor SLSNe (see Table 1 of Gal-Yam 2012).

5. SPECTRA

5.1. Observations

Most of the discussion from here on will focus on SNLS 06D4eu, since unlike SNLS 07D2bv, the host redshift is known, thus allowing fits to spectra and the accurate calculation of energetics.

The spectrum of SNLS 06D4eu was taken at −17 days with respect to U maximum, making it one of the earliest spectra from a SLSN (the time of the spectrum is denoted with an "S" in Figure 3). From our simple expanding blackbody model, we predict $T = 13{,}900$ K at this epoch. Figure 6 shows that continuum of the observed spectrum roughly matches a blackbody at $T = 13{,}500$ K (see Figure 8 for the effect of changing the temperature by ±500 K). This is consistent with the blackbody model and independent verification of the high temperatures reached in the explosion.

As Figure 2 shows, the spectrum of SNLS 06D4eu is quite different from that of other SLSNe. It extends farther into the rest-frame UV, since it was observed at a higher redshift. Features redward of 2200 Å appear depressed in SNLS 06D4eu relative to the other events. SNLS 06D4eu also peaks farther in the UV.

The feature near 2200 Å, seen in SCP 06F6 and PTF09atu, is apparent in SNLS 06D4eu, though at a higher velocity. This feature is tentatively identified as C II by Quimby et al. (2011). In fact, the feature may consist of two separate lines in the former two SNe that are blended, possibly because they are formed at a higher velocity in SNLS 06D4eu. In addition, there is an apparent absorption feature near 2000 Å that was first seen in SCP 06F6 but is now confirmed in SNLS 06D4eu.

At first glance it is not apparent that SNLS 06D4eu is related to the other SNe. However, it is important to remember that they were observed at very different epochs relative to maximum light. Since we have seen from the light curve

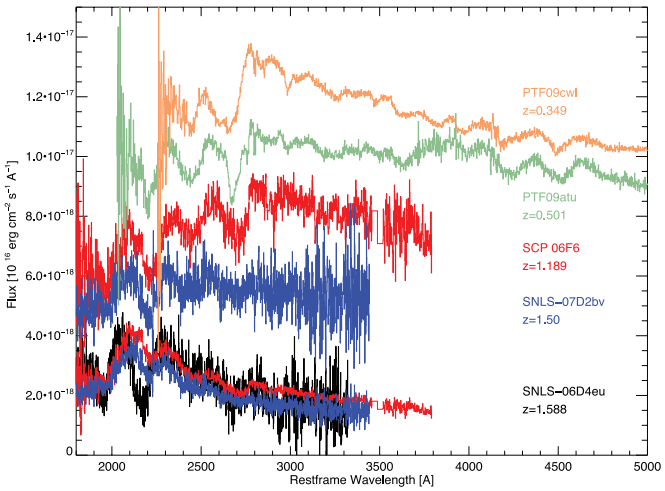

Figure 10. Same as Figure 2 except also showing SCP 06F6 and SNLS 07D2bv dereddened. This is not meant to imply that they are reddened because of dust. Instead, they are redder because they were observed later in phase than SNLS 06D4eu. SCP 06F6 was observed near maximum light in the observer-frame *i* band (Figure 3). SNLS 06D4eu was observed at −17 days relative to rest-frame *U* maximum, when it was hotter. Thus, the relative shallowness of most of the absorption features in SNLS 06D4eu may only be due to the phase of observations. Note, however, that the 2200 Å feature is shallower and has a minimum at a longer wavelength in SCP 06F6. SN features tend to move redward with time as the photosphere recedes inward in mass coordinates as the ejecta expand. The difference may be the result of increased abundance of that element in the outer layers or a different chemical composition between the two supernovae. Alternatively, there is a hint in the spectrum of SCP 06F6 that the line is a blend of two species. If so, higher velocities at early times in SNLS 06D4eu may more effectively blend them.

(A color version of this figure is available in the online journal.)

evolution (Figure 3) that these SNe get dramatically redder as they reach maximum light, to make an appropriate comparison between a spectrum taken at −17 days (SNLS 06D4eu) and one taken near maximum in the observed *i* band, we must deredden the later spectrum. We do this using the IDL astrolib routine CCM_UNRED. The result is shown in Figure 10. Though we use a reddening law to "deredden" the spectra of SCP 06F6 and SNLS 07D2bv, we note that this reddening has nothing to do with dust; it is a natural consequence of an expanding, cooling blackbody.

From Figure 10 it is clear that the differences between SCP 06F6 and SNLS 06D4eu are largely the result of the differing phases at which they were taken. There is an excellent match to the features near 2000 Å, 2500 Å, and 2700 Å. The one feature that does not match as well, the feature at 2200 Å that is possibly C II, is shallower and redder in SCP 06F6. Since the photosphere recedes in mass coordinates with time in a SN, and SN absorption features generally get redder with time as absorption is happening at lower velocities, it is not surprising to see this behavior. In fact, we might ask why we do not see it in the other absorption lines. The relative depth of the 2200 Å feature may be due to differing abundances, distribution, or ionization state of the element or elements that give rise to it, possibly C II.

Since the lines in these SNe are so far in the ultraviolet, they have never been seen before in SNe, making identifications problematic. Quimby et al. (2011) used SYNOW, a parameterized code for line identifications that uses the local thermodynamic equilibrium and other approximations (see Supplementary Information in Quimby et al. 2011). Here we use a full radiative transfer model, which should result in more accurate identifications.

5.2. Theory

To further interpret the spectra and constrain the physical properties of SNLS 06D4eu, we ran synthetic spectrum calculations with the Monte Carlo radiative transfer code SEDONA (Kasen et al. 2006). Rather than using ejecta models based on first-principles explosion simulations, we instead attempt to empirically reproduce the spectra by varying ejecta mass, composition, time since explosion, and total energy in a parameterized way.

The ejecta density structure was assumed to be spherically symmetric and to follow a broken power law (Chevalier & Soker 1989) with a shallow inner region ($\rho \propto v^{-1}$) and a steep outer region ($\rho \propto v^{-8}$). Such a profile is a reasonable approximation to the density structure seen in hydrodynamical models of core-collapse SNe. This model does not, however, capture the possible existence of global asymmetries or clumpiness or the presence of a dense shell due to a magnetar inflated central bubble.

The composition of the ejecta was assumed to be homogeneous. We explored five different abundance distributions: (1) solar, (2) helium-rich, in which all hydrogen in the solar composition was converted into helium, and (3) C/O-rich, in which all the hydrogen and helium in the solar composition was converted to equal parts carbon and oxygen, (4) O–Mg–Ne, in which the composition is taken from the oxygen–magnesium–neon layers of a massive star progenitor from the stellar evolution models of Woosley et al. (2002), and (5) IME burned, in which the intermediate mass elements have been burned, similar to a SN Ia. The first four compositions span the range of possible massive stars depending on how stripped their envelopes are.

We calculated synthetic spectra at fixed snapshots in time, under the stationarity approximation (Jeffery & Branch 1990). Photons were emitted from the surface of an inner spherical boundary, with a total luminosity *L*. The emergent spectrum was fairly insensitive to the location of the inner boundary, as long as it was situated well below the photosphere; we placed the inner boundary at $v_{\rm core} = 5000$ km s^{-1}. The temperature structure above the photosphere was calculated self-consistently under the assumption of radiative equilibrium.

5.3. Analysis

Figure 11 shows the observed spectra of SNLS 06D4eu and SCP 06F6 compared with models of varying luminosity but fixed ejecta mass ($M = 5\ M_{\odot}$), kinetic energy ($E = 10^{52}$ erg), phase (maximum light) and C/O-rich composition. Probable line identifications are marked on the figure lines and are based on determining the lines with the highest Sobolev optical depth (Sobolev 1960) near the photosphere. Firm line identification is difficult given that most features are blends, with the relative strength of the different components varying with luminosity and time.

By using the same mass and composition, but different luminosities for the models in Figure 11, we achieve spectra that look like SCP 06F6 in the least luminous case and like SNLS 06D4eu in the most luminous case. This is consistent with the idea that these SNe are physically related, but SNLS 06D4eu is exceptionally luminous and was seen at an earlier phase where the temperature was higher.

The best-match luminosity for SNLS 06D4eu is $L = 2 \times 10^{44}$ erg s^{-1}, which corresponds to the approximate bolometric

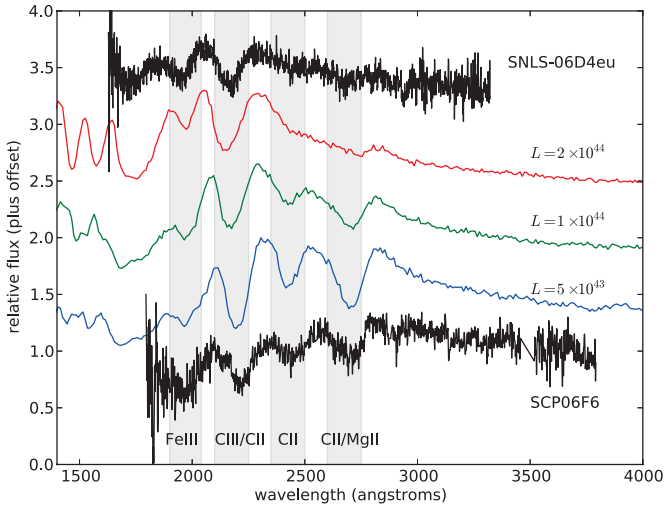

Figure 11. Black: observed spectra of SNLS 06D4eu at −17 days and SCP 06F6 near maximum light. Colored lines: putting different luminosities thorough a model using a 5 $M_{\odot}$ carbon–oxygen progenitor with solar abundances. Lines of Fe III, C III, C II, and Mg II are identified. The data are consistent with SNLS 06D4eu and SCP 06F6 having come from a similar progenitor but having different luminosities, partially due to intrinsic luminosity differences and partially due to them being observed at different phases. Here model spectra are computed at a fixed phase (near maximum light), while the luminosity was varied. Luminosity is given in erg s^{-1}.

(A color version of this figure is available in the online journal.)

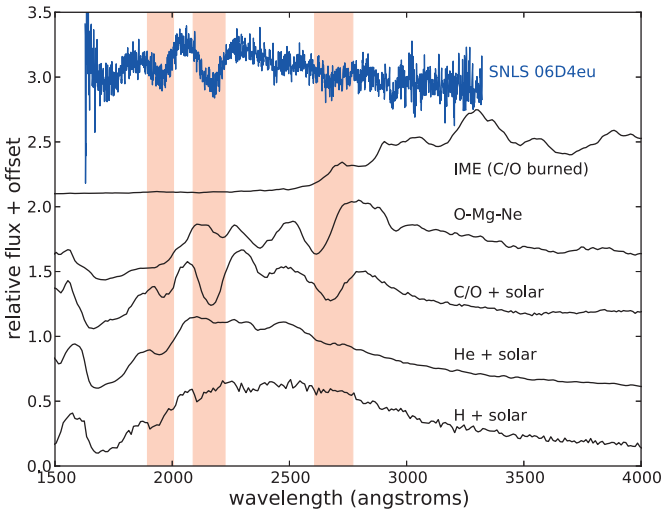

Figure 12. Synthetic spectra for models with different ejecta abundances. Each model has an ejecta mass of $M = 5\ M_{\odot}$ and kinetic energy of $E = 10$ B (B = Bethe, 10^{51} erg). The spectral features of SNLS 06D4eu are best fit by a model composed of carbon and oxygen with a solar abundance of other elements. The IME (C/O burned) model is one in which the carbon and oxygen is burned to intermediate mass elements, similar to a Type Ia supernova.

(A color version of this figure is available in the online journal.)

luminosity at the time the spectrum was observed (17 days before maximum light). In subsequent calculations, we fix the luminosity at this value.

Note that in Figure 11, in the interest of varying only one parameter, the luminosity was changed, while the phase was fixed at maximum light. While this phase is appropriate for SCP 06F6, SNLS 06D4eu was observed 17 days before maximum light. Fortunately, the model is not very sensitive to the assumed time from explosion. In subsequent calculations for SNLS 06D4eu, we adopt a phase of 25 days since explosion for the date of the spectrum. Taken at face value, the simple blackbody model had a rise time of 30 days, so day −17 corresponds to 13 days after explosion (Figure 9). However, the spectral fit is not quite as good at day 13 after explosion. In particular, the Fe III feature at 2000 Å is not as well fit. This is because Fe III is mostly ionized at these early epochs due to the high photospheric temperatures. Since it is clear from the earliest light curve points that the simple blackbody model is a poor approximation at early times, this date of 13 days since explosion cannot be taken too seriously. The observations before −30 days are limits, so the true explosion time is unconstrained. Many other SNe of this class have longer rise times than 30 days, some as long as 60 days (Figures 3 and 7). Therefore, we adopt the longer 42 day rise (making the day −17 spectra correspond to 25 days after explosion) for all subsequent spectroscopic models of SNLS 06D4eu.

The reasonable fit of the fiducial model Figure 11 provides strong evidence that the ejecta of SNLS 06D4eu was rich in carbon and oxygen. We identify the 2000 Å feature as Fe III, the 2200 Å feature as C III and C II, the 2400 Å feature as C II, and the 2700 Å feature as Mg II and C II. In contrast, Quimby et al. (2011) had identified the 2200 Å feature as C II, the 2400 Å feature as Si III, and the 2700 Å feature as Mg II. They did not identify a feature at 2000 Å. If the feature at 2200 Å is indeed C III, then its strength may be a result of the relatively high temperatures seen at this phase in SNLS 06D4eu.

Figure 12 shows that if the composition is instead assumed to be hydrogen, helium, O–Mg–Ne, or intermediate mass element rich, none of the major spectral features are reproduced. When we pair our finding that carbon is required to reproduce the UV spectra of SLSNe with the previous finding of Quimby et al. (2011) that the most prominent lines in the optical are O II, we get a picture of the nature of the SLSN ejecta as one dominated by C and O. We therefore associate SNLS 06D4eu with the class of Type Ic supernovae (SNe Ic) presumed to be the explosions of the C/O cores of stripped envelope massive stars. This is consistent with the finding of Pastorello et al. (2010), who found an empirical connection between the later-time spectra of SLSNe and SNe Ic.

As seen in Figure 12, the spectra of models with the H- and He-rich composition are largely featureless, with only a few broad features that can be attributed to the solar abundance of metals. No conspicuous lines of H and He are seen, even though these elements are the dominant constituent of the atmosphere. This is because all H and He lines in the observed wavelength range turn out to be weak given the ionization and excitation conditions in the high temperature atmosphere. As a result, we cannot definitively rule out that the ejecta of SNLS 06D4eu contained some amount of H and He that is simply not visible in the spectrum. However, any layer rich in H or He would have to exist at high velocities ($\gtrsim$20,000 km s^{-1}) well above the photospheric layer rich in C–O that is seemingly required to produce the line features that are seen in the spectrum.

It is difficult to constrain the mass and energetics of SNLS 06D4eu only on the basis of the spectral fit. However, the high Doppler shifts suggest a high kinetic energy. For $M = 5\ M_{\odot}$, we need $E = 10$ B to reproduce the blueshifts of the features (Figure 13). Thus, it was a hyperenergetic SN. Since the total radiated energy was 1 B, this also indicates that these SNe radiate energy much more efficiently than a typical core-collapse SN, where the radiated energy is 1% of the kinetic energy.

While some studies have speculated that SLSNe result from the explosion of very massive stars, here a model with only 5 $M_{\odot}$ of ejecta was sufficient to explain the spectra. While

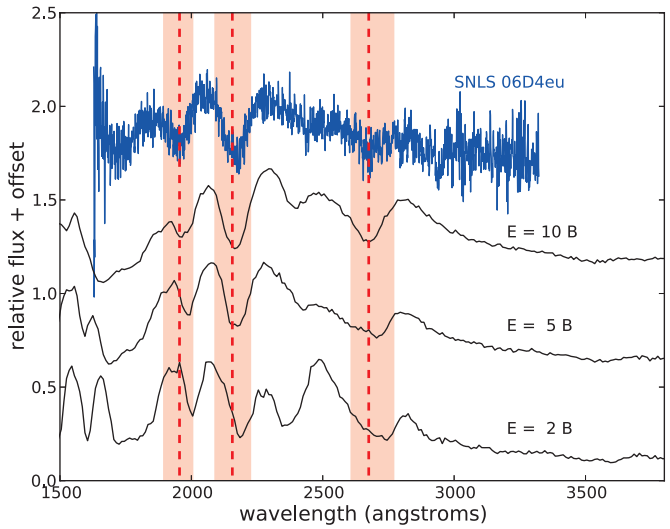

Figure 13. Synthetic spectra for models with different kinetic energies. Each model has a C/O-rich composition and ejecta mass $M = 5\ M_{\odot}$. Dashed lines show the approximate minimum of the absorption features in the observed spectrum, while shaded regions show the extent of the feature. The model with $E = 10$ B best reproduces the blueshifts of the features. Thus, we require a model with relatively high explosion energy, $E/M \sim 2$ B $M_{\odot}^{-1}$.

(A color version of this figure is available in the online journal.)

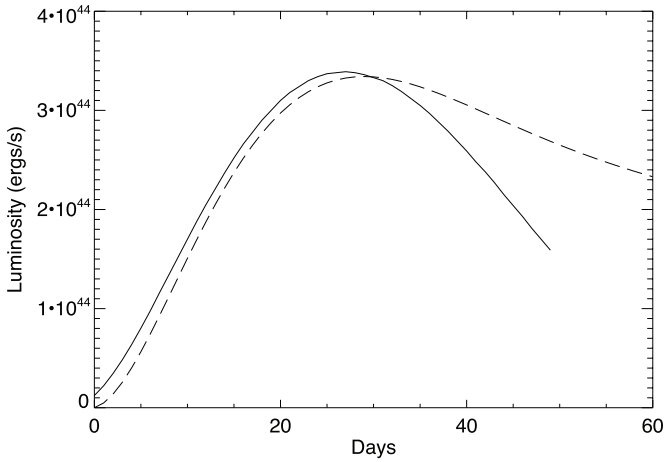

Figure 14. Can ^{56}Ni decay power the light curve of SNLS 06D4eu? The solid line shows the bolometric light curve of SNLS 06D4eu derived from the blackbody fit. Days are in the rest frame, and day 30 corresponds to the fiducial peak in the observed i band of MJD = 54020 (day 0 in most other plots). The peak of the blackbody curve is at 26.5 days, or 3.5 rest-frame days before the fiducial "day 0." The dashed line is the simple parameterized model of Chatzopoulos et al. (2009) with a rise time of 25 days, $v = 12{,}000$ km s^{-1} (to match the observed spectra), $\kappa = 0.1$, $M_{\rm Ni} = 23.5\ M_{\odot}$, and $M_{\rm ej} = 25\ M_{\odot}$. A very large mass of ^{56}Ni is required to explain the extreme luminosity, but such a large ejecta mass also requires a long diffusion time and slowly declining light curve. No reasonable choice of parameters in this model can match the relatively fast decline of SNLS 06D4eu.

a much higher ejecta mass ($\sim$100 $M_{\odot}$) cannot be ruled out on the basis of the spectrum alone, given the high observed velocities such a model would require an extremely large energy, $\gtrsim$100 B. In Section 6 we will investigate the mass of the required progenitor needed to match the observed light curve.

6. LUMINOSITY

The physical mechanism powering extreme SNe like SNLS 06D4eu is unclear, as the normal core-collapse process does not provide the requisite 10^{51} erg of radiated energy. However, there are some constraints any physical mechanism must meet, including peak output in the ultraviolet, temperatures in excess of 15,000 K, a 20–50 day rise and similar decline, and a spectrum devoid of hydrogen but rich in C, O, Fe, and Mg. Here we discuss the hypothesized power sources and explosion mechanisms.

6.1. ^{56}Ni *Decay*

SNe Ia are powered by the radioactive decay of ^{56}Ni. In the thermonuclear destruction of a white dwarf, up to a solar mass or more of ^{56}Ni is synthesized, and its decay to ^{56}Co and ultimately ^{56}Fe releases gamma-ray photons that are reprocessed and ultimately diffuse out of the ejecta at UV–optical–IR wavelengths, reaching a peak luminosity in about 3 weeks (Arnett 1982). However, SNLS 06D4eu is more than 10 times as bright as a typical SN Ia. Could it still be powered by ^{56}Ni?

We use the prescription in Chatzopoulos et al. (2009) to calculate a simple model light curve expected from ^{56}Ni decay (Figure 14). A constant opacity of $\kappa = 0.1$ (appropriate for a non-hydrogen atmosphere) is used, as is an ejecta velocity of 12,000 km s^{-1}, measured from the spectra. To fit the extreme luminosity of SNLS 06D4eu, a ^{56}Ni mass of $M_{\rm Ni} = 23.5\ M_{\odot}$ is required. Such a large mass of material requires a long time for photons to diffuse out. Even for an ejecta mass of $M_{\rm ej} = 25 M_{\odot}$ (i.e., only 1.5 $M_{\odot}$ of nonradioactive material), the fall time of the model light curve cannot be made to match the more rapid decline of the bolometric light curve. Furthermore, such a large ball of ^{56}Ni, with only a small layer of other material necessary to reproduce the spectrum, seems implausible.

6.2. *Pair Instability*

Theoretically, very high mass stars ($M \gtrsim 100\ M_{\odot}$) with a core mass above $\sim$50 $M_{\odot}$ ought to achieve such high temperatures that electron–positron pairs are created, decreasing pressure support in the core, which is followed by core contraction, oxygen ignition, a large amount of synthesized radioactive nickel, and an explosion that disrupts the star (Barkat et al. 1967). This pair instability mechanism has been invoked to explain the superluminous supernova SN 2007bi (Gal-Yam et al. 2009), especially its large luminosity, slowly declining light curve matching ^{56}Co decay, and nebular spectra implying a large core and nickel mass. It may explain other SNe as well (see Gal-Yam 2012 for a review). However, Moriya et al. (2010) present an alternative, standard core-collapse model for SN 2007bi, albeit a massive one ($\sim$100$M_{\odot}$) that ejects 6.1 $M_{\odot}$ of ^{56}Ni.

Despite its large luminosity, the pair instability model does not seem to fit SNLS 06D4eu. As indicated in the previous section, the relatively fast decline of SNLS 06D4eu argues against a large ^{56}Ni mass. The spectra of SNLS 06D4eu and other similar objects are also distinct from that of SN 2007bi.

6.3. *Interaction*

The class of SNe known as SNe IIn (Type II supernovae with narrow hydrogen lines in their spectra) can occasionally reach luminosities in the realm of that seen here (see Neill et al. 2011). This is because extra energy is injected well after the SN has expanded from its initial radius by the collision of the ejecta with preexisting CSM. This interaction produces relatively narrow emission lines of hydrogen because of the slow speed of the CSM. Often this line is superimposed on a broader line of order hundreds to thousands of kilometers per

second. Absorption lines are generally absent, and a featureless blue continuum may dominate at early times. Furthermore, interaction generally powers the light curve for many tens to hundreds of days, keeping it from showing a strong decline over this time period. None of the typical features of SNe IIn match the observations of SNLS 06D4eu, so we conclude that it is not likely to be interacting with previously cast-off circumstellar hydrogen from the progenitor.

Could it be possible that SNLS 06D4eu and SNe like it are powered by interaction with something other than hydrogen? To explain PTF10iue, an SN Ic with a very slowly declining light curve but no narrow lines of hydrogen, Ben-Ami et al. (2013) posit that it is a stripped-envelope SN interacting with a clumpy, hydrogen-free circumstellar medium. This would explain the narrow high-density oxygen emission lines seen in its spectrum and its unusually slowly declining light curve, which had a plateau in the r band for ~200 days and declined less than 3 mag over 500 days. But SNLS 06D4eu, SNLS 07D2bv, and similar SLSNe do not have slowly declining light curves nor do they show narrow emission lines of any element. It would take an extraordinary degree of fine-tuning to create CSM that was fast-moving enough not to form narrow lines, was at the right density and morphology to increase the SN luminosity, but not dilute the spectra, and was perfectly situated to avoid a plateau in the light curve.

6.4. Pulsational Pair Instability

Quimby et al. (2011) found that one way to achieve the high luminosities in SLSNe is to invoke an injection of energy at a radius of about 10^{15} cm, possibly though interaction with CSM. However, since the SLSNe spectra are dominated by elements such as C, O, Fe, and Mg and narrow lines of hydrogen are nowhere to be found, the normal mechanism powering an SN IIn, would appear not to be at work. Another possibility is the collision of fast-moving shells made of heavier elements that may be present in the hypothesized pulsational pair-instability SNe (Woosley et al. 2007). These are theoretically predicted to arise in the deaths of massive stars where pulsations initially do not succeed in destroying the star but instead eject shells of material. The interaction at a large radius would overcome the problem of adiabatic losses, the lack of hydrogen could be explained if there was either previous mass loss or if the initial pulses rid the star of hydrogen, and the lack of narrow lines would be explained by the relatively high velocity of ejected material. For example, in the 25 $M_{\odot}$ model of Woosley et al. (2007), the initial pulsation produces an outburst of $\sim 6 \times 10^{41}$ erg s^{-1}, lasting 200 days. Subsequent interaction occurs 7 yr later, reaching luminosities of a few $\times 10^{43}$ erg s^{-1}. The final iron core-collapse then happens after another 9 yr.

While the pulsational pair-instability SN model offers advantages, it requires fine-tuning. As noted in the previous section, shells must be perfectly placed to add luminosity (without a plateau) and avoid effects in the spectra. Such a model would in fact be different than the initially presented pulsational pair-instability model, which assumed a star with outer layers of hydrogen. Further work must be done to create detailed predictions of light curves and spectra from the model in an attempt to match SLSNe. One prediction is that precursor explosions might be observable. In the 25 $M_{\odot}$ model of Woosley et al. (2007) mentioned above, they would be more than 6 mag fainter than the peak of SNLS 06D4eu. At $z = 1.588$ we have little hope of having seen them. Note, however, a precursor outburst was seen 40 days before a SN in SN 2010mc/PTF10tel (Ofek et al. 2013). It was 4 mag fainter than the peak. The subsequent SN was an SN IIn.

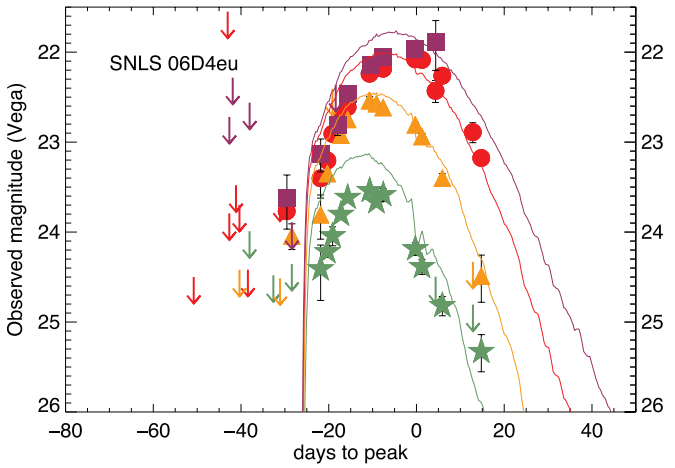

Figure 15. 06D4eu $griz$ photometry compared with theoretical light curves from a magnetar spin-down model. The model was derived from the initial work of Kasen & Bildsten (2010). This best-fit model has a mass of 3 $M_{\odot}$, a magnetic field of $B = 2 \times 10^{14}$ G, and an initial period of $P = 2$ ms. A better fit could be achieved with fine-tuning.

(A color version of this figure is available in the online journal.)

6.5. Creation and Spin-down of a Magnetar

Woosley (2010) and Kasen & Bildsten (2010) hypothesize that the creation and spin-down of a magnetar may be able to inject enough energy at late times into a SN to account for the extreme luminosity of SLSNe. The tunable parameters in this model are the mass of the progenitor, the size of the magnetic field, and the starting spin rate of the newly formed neutron star. In Figure 15 we compare the light curves of SNLS 06D4eu with such a model by using a 3 $M_{\odot}$ progenitor, a magnetic field 2×10^{14} G, and an initial period of $P = 2$ ms. From Equation (2) of Kasen & Bildsten (2010), the spin-down timescale is 24 days. This was one of a grid of precomputed models without reference to SNLS 06D4eu; fine-tuning could improve the fit.

The model succeeds in matching the overall luminosity, rise and fall time, and rough flux distribution in $griz$ for SNLS 06D4eu. The match to the fall time is particularly notable, since SNe with evidence for interaction tend to have long plateaus, and models with the required amount of ^{56}Ni also have a long fall time. This is possible because of the relatively small size of the progenitor, 3 $M_{\odot}$. Furthermore, a comparably sized progenitor (5 $M_{\odot}$) made of carbon and oxygen can reproduce the spectra (Figure 11) of not only SNLS 06D4eu but also SLSNe in general.

Still, questions remain. It is also not known how the energy of the spin-down is coupled to the expanding ejecta. And these models are still relatively primitive—the spectra model and the light curve models are not self-consistent, nor do they contain explosion physics. They also have several free parameters that can be tuned over a wide range. Other possible limitations of the model include that it does not necessarily predict that the progenitors should be hydrogen-free, nor does it address the preference for dwarf hosts. It may be that more massive stars produce SNe Ic or that mass loss is associated with metal-poor hosts.

6.6. Accretion-driven SNe

Another possibility is an engine-driven SN, like those thought to occur in hypernovae. For example, one can imagine a jet

injecting energy into expanding ejecta at late times, achieving the same result as that in the magnetar spin-down model. Since few detailed models exist, we can only discuss the broadest of implications for this idea. Pastorello et al. (2010) linked hydrogen-poor SLSNe to SNe Ic, though the velocities seen here, 12,000 km s^{-1}, are not as high as those seen in the broad-lined SNe Ic linked to GRBs.

Gamma-ray bursts do favor low-metallicity dwarf hosts (Modjaz et al. 2008). But Arcavi et al. (2010) find that normal SNe Ic are disfavored in dwarf galaxies, which tend to produce either SNe Ib or broad-lined SNe Ic instead. They hypothesize that metallicity-driven mass loss strips SNe enough to become a normal SN Ic only in relatively metal-rich environments. This fits with the finding that the sites of SNe Ic are more metal-rich than those of SNe Ib (Modjaz et al. 2011). It is unclear how hydrogen-deficient SLSNe would fit into this picture.

Dexter & Kasen (2013) consider an accretion-powered scenario, in which some of the ejecta remains bound, falls back on the newly created neutron star or black hole, and then drives an outflow (a jet or disk wind) that reenergizes the outgoing ejecta at relatively late times (∼weeks). While they used progenitors that matched those of SNe Ic, they were unable to match the luminosities seen in SNLS 06D4eu. However, the model is still in its early stages, and the assumptions about accretion efficiency were relatively conservative.

The accretion model may be observationally difficult to distinguish from the magnetar model; both involve some central energy source. The one main difference may be that the magnetar power likely continues until late times (with a t^{-2} tail from spin-down), while it is possible that accretion onto the black hole could suddenly cease at some point (if the black hole is powerful enough to blow away all of the infalling material). So the black hole model could explain a sharply falling light curve at later times (without a tail), while this would be hard to explain with a magnetar. We do not have the late-time data here to distinguish between the models. However, Inserra et al. (2013) do favor the magnetar model for SLSNe on the basis of late-time light curves.

7. CONCLUSIONS

As the most distant SLSN with a spectrum ($z = 1.588$), SNLS 06D4eu provides a rare glimpse of the chemical composition and light curve evolution of an early-universe SN. It is also one of the most luminous SNe known, reaching $M_U = -22.7$ at peak with a luminosity of 3.4×10^{44} erg s^{-1}, 10^{51} erg total radiated energy, and an explosion energy of 10^{51} erg. It is unlike a traditional core-collapse, thermonuclear or interaction-powered SN, but it is similar to the emerging class of SLSNe that do not have hydrogen in their spectra (Gal-Yam 2012).

SNLS 07D2bv is another similar SN, with $griz$ light curves that rise and fall on a similar timescale and that start out blue and become redder over time. While its redshift is not known with certainty, it is likely at $z \sim 1.5$ on the basis of a match to SNLS 06D4eu. If so, it is ∼1 mag dimmer than SNLS 06D4eu. Its spectrum is similar to that of SNLS 06D4eu, albeit redder, which is consistent with it being taken ∼1 week (rest frame) later.

Only a handful of SLSNe are known, so their ensemble properties are not yet fully understood. Indeed, there is considerable uncertainty about where to draw the boundaries between SLSNe with different properties. The fact that two SNe show such striking similarities and match a subset of other known SLSNe points to a common origin. These two SNe provide the first detailed look into the rest-frame ultraviolet of these SNe, where they radiate most of their energy. In addition, they are the most complete light curve of a SLSN in multiple bands, stretching from well before maximum light to past maximum.

The spectra presented here are some of the earliest, bluest spectra of these events, taken 17 days (06D4eu) and 10 days (07D2bv) before rest-frame U-band maximum. They bear similarity to one of the other SLSNe with a rest-frame ultraviolet spectrum, PTF09atu, but are apparently hotter and are dominated by two strong absorption lines between 1700 and 2000 Å that we identify as a blend of C III and C II and Fe III. Other lines, C II and a blend of C II and Mg II, are weak in SNLS 06D4eu but are more apparent in the first identified SLSN, SCP 06F6.

According to our model, these lines should be weaker at higher luminosities, which is consistent with the extreme luminosity of SNLS 06D4eu. By fitting a simple blackbody model to the light curve of SNLS 06D4eu, we find temperatures initially in excess of 15,000 K, dropping by about 200 K day^{-1}. At the time the spectrum was taken, the SN was between 13,000 and 14,000 K. This accounts for some of the strange ionization states, such as C III, rarely seen in SNe.

The host galaxy redshift of SNLS 06D4eu of $z = 1.588$ was determined from VLT X-Shooter observations taken after the SN had faded. Using X-Shooter, we were able to detect host lines of Hα, Hβ, O II, O III, and N II. From this we determined that the host of SNLS 06D4eu is forming stars at a rate of approximately 8 $M_\odot$ yr^{-1} and has a metallicity between solar and one-quarter solar. These findings are consistent with those of Neill et al. (2011), who found that similar SNe Ia are preferentially found in UV-bright hosts that are often low mass and possibly slightly metal-poor.

We can reproduce the day −17 spectrum of SNLS 06D4eu with a model with 5 $M_\odot$ ejecta, total energy $E = 10$ B, C/O plus solar composition, bolometric luminosity 2×10^{44} erg s^{-1}, and a phase approximately 25 days after explosion. A high luminosity is required to reproduce the blue spectra and ionization states seen, a low mass is required to produce the rapid rise and fall of the light curve, and high kinetic energy are required to reproduce the blueshifts of the features. When combined with the C/O composition, from a progenitor perspective, these SLSNe appear to be related to SNe Ic.

The mechanisms powering normal SNe as presently understood—radioactive decay, the prompt injection of the energy of gravitational collapse into a stellar envelope, or the interaction of a SN with hydrogen-rich CSM—cannot explain the extreme energies and lack of hydrogen seen in SNLS 06D4eu and similar events. Models invoking a massive generation of ^{56}Ni would require 23.5 $M_\odot$ to be synthesized, and with so much ejecta, they cannot reproduce the relatively rapid light curve decay of SNLS 06D4eu. Therefore, the pair-instability model invoked for SN 2007bi (Gal-Yam et al. 2009) would not seem to be viable.

The magnetar spin-down model of Kasen & Bildsten (2010) (see also Woosley 2010), with an initial period of 2 ms, a magnetic field of 2×10^{14} G, and a progenitor of 3 $M_\odot$ can account for the total energy required and can match the general rise, fall, and color behavior of SNLS 06D4eu. However, this model offers no particular explanation for the hydrogen-poor nature of these SNe or their predominance in high-star-forming, possibly metal-poor galaxies.

On the other hand, the pulsational pair-instability model (Woosley et al. 2007) may address the lack of hydrogen if it was lost in a previous outburst, and it could explain the preference for a high-star-forming, UV-bright environment if a massive progenitor is required. However, detailed spectroscopic and light curve predictions have yet to be performed for the model. Engine-driven SNe, where a jet injects energy at late times, could also achieve the high luminosities seen in SLSNe, but in the absence of sophisticated models, this remains speculative. Alternatively, these SNe could be the result of a process not yet imagined.

It is ironic that the brightest SNe known have been missed by observers for centuries. Partly this is because of their rarity: they may make up only 1 in 10,000 SNe (Quimby et al. 2013). But another reason is that, with their peak output in the UV, Earth-bound observers have been missing most of the action. Finally, a third reason may be their predominance in highly star-forming and possibly metal-poor galaxies. These environments would have been common in the early universe, where the SFR was an order of magnitude higher than it is today and the buildup of metals had not yet reached present-day levels. It is possible that SNLS 06D4eu is a relic of an earlier form of SNe that is all but extinct today.

The future holds great promise for probing these mysterious events in detail. Surveys like the intermediate PTF (Kulkarni 2013) and LaSilla/QUEST (Baltay et al. 2013) are surveying large volumes of sky at low redshift (the volume surveyed for these luminous events is much higher) and finding several per year. But to understand these SNe, we need to observe them extensively in the rest-frame ultraviolet, where they radiate their peak energies. For this, higher-redshift surveys like Pan-STARRS (Chomiuk et al. 2011) and the Dark Energy Survey (Bernstein et al. 2012) are well suited.

D.A.H. acknowledges support from LCOGT. C. Lidman acknowledges the support provided by the Oskar Klein Center at the University of Stockholm. Based on observations obtained with MegaPrime/MegaCam, a joint project of CFHT and CEA/DAPNIA, at the Canada–France–Hawaii Telescope (CFHT), which is operated by the National Research Council (NRC) of Canada, the Institut National des Science de l'Univers of the Centre National de la Recherche Scientifique (CNRS) of France, and the University of Hawaii. Based in part on observations taken at the ESO Paranal Observatory (ESO programs 176.A-0589 and 384.D-0222). C.P. and R.C. acknowledge financial support from the Natural Sciences and Engineering Research Council of Canada. This work was supported in part by French state funds managed by the ANR within the Investissements d'Avenir program under reference ANR-1-IDEX-0005-02.

Facilities: VLT:Antu (FORS1), VLT:Kueyen (X-Shooter), CFHT (Megacam)

REFERENCES

Arnett, W. D. 1982, ApJ, 253, 785
Arcavi, I., Gal-Yam, A., Kasliwal, M. M., et al. 2010, ApJ, 721, 777
Balland, C., Baumont, S., Basa, S., et al. 2009, A&A, 507, 85
Baltay, C., Rabinowitz, D., Hadjiyska, E., et al. 2013, PASP, 125, 683
Barbary, K., Dawson, K. S., Tokita, K., et al. 2009, ApJ, 690, 1358
Barkat, Z., Rakavy, G., & Sack, N. 1967, PhRvL, 18, 379
Ben-Ami, S., Gal-Yam, A., Mazzali, P. A., et al. 2013, arXiv:1309.6496
Bernstein, J. P., Kessler, R., Kuhlmann, S., et al. 2012, ApJ, 753, 152
Bielby, R. M., Finoguenov, A., Tanaka, M., et al. 2010, A&A, 523, A66
Bronder, T. J., Hook, I. M., Astier, P., et al. 2008, A&A, 477, 717
Chatzopoulos, E., Wheeler, J. C., & Vinko, J. 2009, ApJ, 704, 1251
Chevalier, R. A., & Soker, N. 1989, ApJ, 341, 867
Chomiuk, L., Chornock, R., Soderberg, A. M., et al. 2011, ApJ, 743, 114
Conley, A., Guy, J., Sullivan, M., et al. 2011, ApJS, 192, 1
Dexter, J., & Kasen, D. 2013, ApJ, 772, 30
D'Odorico, V., Viel, M., Saitta, F., et al. 2006, MNRAS, 372, 1333
Ellis, R. S., Sullivan, M., Nugent, P. E., et al. 2008, ApJ, 674, 51
Gal-Yam, A. 2012, Sci, 337, 927
Gal-Yam, A., Mazzali, P., Ofek, E. O., et al. 2009, Natur, 462, 624
Guy, J., Sullivan, M., Conley, A., et al. 2010, A&A, 523, A7
Howell, D. A., Sullivan, M., Perrett, K., et al. 2005, ApJ, 634, 1190
Inserra, C., Smartt, S. J., Jerkstrand, A., et al. 2013, ApJ, 770, 128
Jeffery, D. J., & Branch, D. 1990, in Supernovae, Jerusalem Winter School for Theoretical Physics, ed. J. C. Wheeler, T. Piran, & S. Weinberg (Singapore: World Scientific), 149
Kasen, D., & Bildsten, L. 2010, ApJ, 717, 245
Kasen, D., Thomas, R. C., & Nugent, P. 2006, ApJ, 651, 366
Kennicutt, R. C. 1998, ARA&A, 36, 189
Kewley, L. J., & Ellison, S. L. 2008, ApJ, 681, 1183
Kim, A., Goobar, A., & Perlmutter, S. 1996, PASP, 108, 190
Kobulnicky, H. A., & Kewley, L. J. 2004, ApJ, 617, 240
Kulkarni, S. R. 2013, ATel, 4807, 1
Law, N. M., Kulkarni, S. R., Dekany, R. G., et al. 2009, PASP, 121, 1395
Leloudas, G., Chatzopoulos, E., Dilday, B., et al. 2012, A&A, 541, A129
McMahon, R. 2012, in Science from the Next Generation Imaging and Spectroscopic Surveys, ESO Garching, 2012 October 15–18
Modjaz, M., Kewley, L., Bloom, J. S., et al. 2011, ApJL, 731, L4
Modjaz, M., Kewley, L., Kirshner, R. P., et al. 2008, AJ, 135, 1136
Moriya, T., Tominaga, N., Tanaka, M., Maeda, K., & Nomoto, K. 2010, ApJL, 717, L83
Neill, J. D., Sullivan, M., Gal-Yam, A., et al. 2011, ApJ, 727, 15
Ofek, E. O., Sullivan, M., Cenko, S. B., et al. 2013, Natur, 494, 65
Osterbrock, D. E. 1989, Astrophysics of Gaseous Nebulae and Active Galactic Nuclei (Mill Valley, CA: University Science Books)
Pagel, B. E. J., Edmunds, M. G., Blackwell, D. E., Chun, M. S., & Smith, G. 1979, MNRAS, 189, 95
Pastorello, A., Smartt, S. J., Botticella, M. T., et al. 2010, ApJL, 724, L16
Perrett, K., Balam, D., Sullivan, M., et al. 2010, AJ, 140, 518
Quimby, R. M., Aldering, G., Wheeler, J. C., et al. 2007, ApJL, 668, L99
Quimby, R. M., Kulkarni, S. R., Kasliwal, M. M., et al. 2011, Natur, 474, 487
Quimby, R. M., Yuan, F., Akerlof, C., & Wheeler, J. C. 2013, MNRAS, 431, 912
Sobolev, V. V. 1960, Moving Envelopes of Stars (Cambridge: Harvard Univ. Press)
Sullivan, M., Guy, J., Conley, A., et al. 2011, ApJ, 737, 102
Walker, E. S., Hook, I. M., Sullivan, M., et al. 2011, MNRAS, 410, 1262
Woosley, S. E. 2010, ApJL, 719, L204
Woosley, S. E., Blinnikov, S., & Heger, A. 2007, Natur, 450, 390
Woosley, S. E., Heger, A., & Weaver, T. A. 2002, RvMP, 74, 1015
Yaron, O. 2012, PASP, 124, 668